AD-A043 501 STANFORD RESEARCH INST MENLO PARK CALIF F/G 20/14
VLF/LF PROPAGATION BENEATH IRREGULARLY PERTURBED IONOSPHERES.(U)
JAN 77 G H PRICE, V E HATFIELD DNA001-76-C-0252
UNCLASSIFIED DNA-4250F NL

1 OF 1
AD A043501

END
DATE FILMED
9-77
DDC

AD A043501

DNA 4250F

VLF/LF PROPAGATION BENEATH IRREGULARLY PERTURBED IONOSPHERES

Stanford Research Institute
333 Ravenswood Avenue
Menlo Park, California 94025

January 1977

Final Report for Period 29 March 1976—30 November 1976

CONTRACT No. DNA 001-76-C-0252

APPROVED FOR PUBLIC RELEASE;
DISTRIBUTION UNLIMITED.

DDC
RECEIVED
AUG 30 1977
C

THIS WORK SPONSORED BY THE DEFENSE NUCLEAR AGENCY
UNDER RDT&E RMSS CODE B322076464 S99QAXHB04216 H2590D.

DDC FILE COPY

Prepared for
Director
DEFENSE NUCLEAR AGENCY
Washington, D. C. 20305

Destroy this report when it is no longer needed.
Do not return to sender.

UNCLASSIFIED

SECURITY CLASSIFICATION OF THIS PAGE *(When Data Entered)*

REPORT DOCUMENTATION PAGE

READ INSTRUCTIONS BEFORE COMPLETING FORM

1. REPORT NUMBER: DNA 4250F	2. GOVT ACCESSION NO.
3. RECIPIENT'S CATALOG NUMBER	
4. TITLE *(and Subtitle)*: VLF/LF PROPAGATION BENEATH IRREGULARLY PERTURBED IONOSPHERES	5. TYPE OF REPORT & PERIOD COVERED: Final Report for Period 29 Mar 76—30 Nov 76
	6. PERFORMING ORG. REPORT NUMBER: SRI Project 5056
7. AUTHOR(s): Gary H. Price, V. Elaine Hatfield	8. CONTRACT OR GRANT NUMBER(s): DNA 001-76-C-0252
9. PERFORMING ORGANIZATION NAME AND ADDRESS: Stanford Research Institute, 333 Ravenswood Avenue, Menlo Park, California 94025	10. PROGRAM ELEMENT, PROJECT, TASK AREA & WORK UNIT NUMBERS: NWED Subtask S99QAXHB042-16
11. CONTROLLING OFFICE NAME AND ADDRESS: Director, Defense Nuclear Agency, Washington, D.C. 20305	12. REPORT DATE: January 1977
	13. NUMBER OF PAGES: 48
14. MONITORING AGENCY NAME & ADDRESS *(if different from Controlling Office)*	15. SECURITY CLASS *(of this report)*: UNCLASSIFIED
	15a. DECLASSIFICATION DOWNGRADING SCHEDULE

16. DISTRIBUTION STATEMENT *(of this Report)*

Approved for public release; distribution unlimited.

17. DISTRIBUTION STATEMENT *(of the abstract entered in Block 20, if different from Report)*

18. SUPPLEMENTARY NOTES

This work sponsored by the Defense Nuclear Agency under RDT&E RMSS Code B322076464 S99QAXHB04216 H2590D.

19. KEY WORDS *(Continue on reverse side if necessary and identify by block number)*

VLF/LF Progagation
Nuclear Effects
Scattering from Rough Surfaces
Irregularly Perturbed Ionospheres

20. ABSTRACT *(Continue on reverse side if necessary and identify by block number)*

The disturbance to very-low-frequency and low-frequency propagation produced by numbers of large-yield, low-altitude nuclear detonations is considered. The consequent lower-ionospheric irregularity both reduces the coherent reflection and produces an incoherently scattered component of the signal. These effects are found to be appreciable at detonation densitites in the range of those considered in conjunction with large-scale attack scenarios.

DD FORM 1 JAN 73 1473 EDITION OF 1 NOV 65 IS OBSOLETE

UNCLASSIFIED

SECURITY CLASSIFICATION OF THIS PAGE *(When Data Entered)*

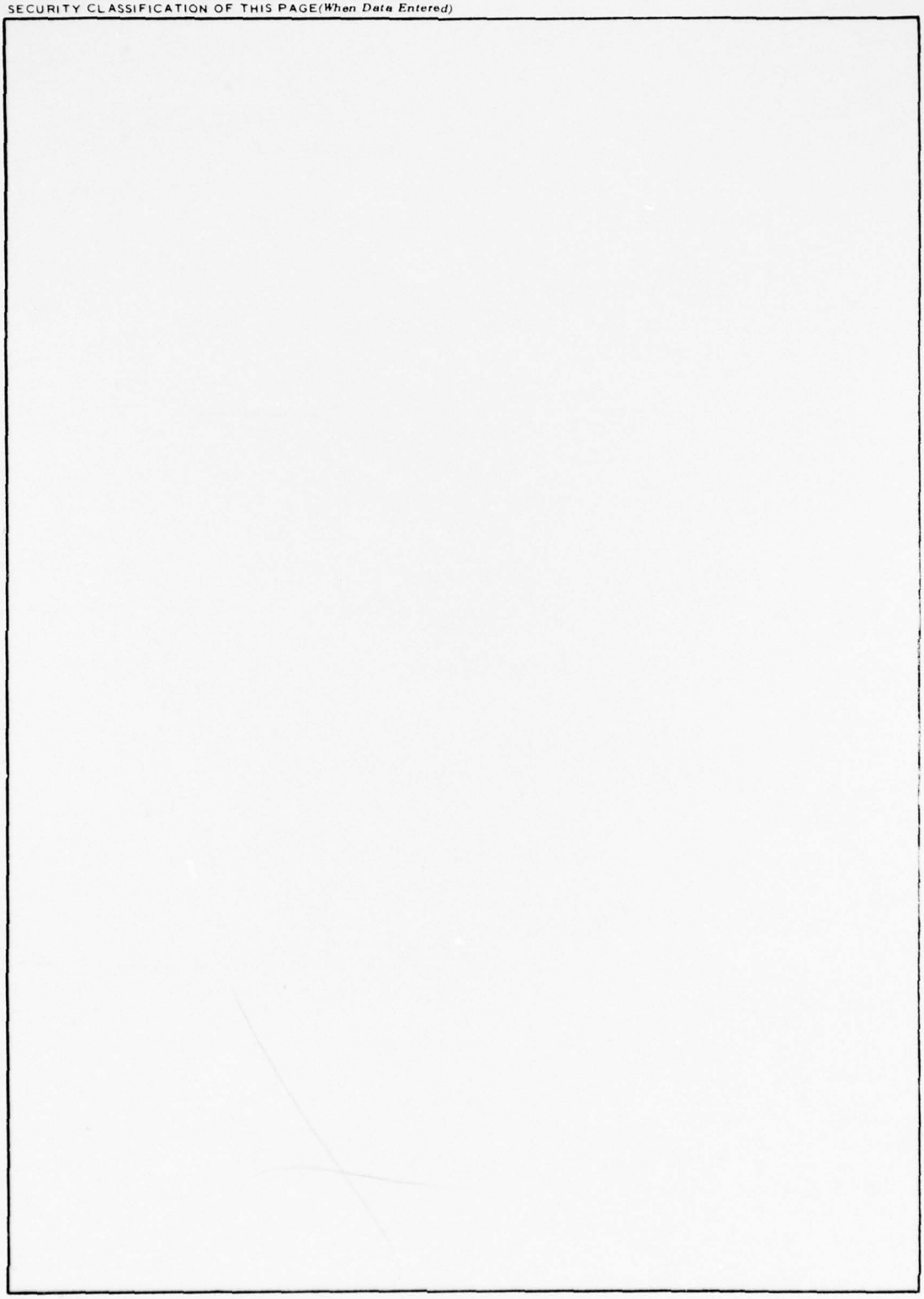

CONTENTS

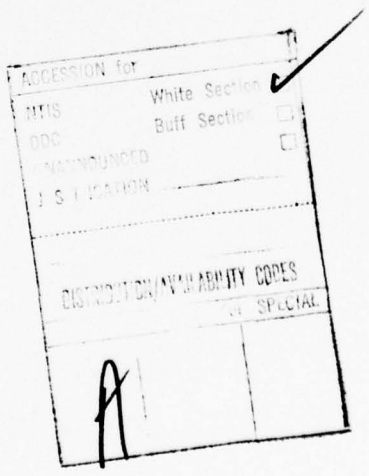

LIST OF ILLUSTRATIONS

LIST OF TABLES

I INTRODUCTION

Evaluation of the expected performance of communications systems, such as the World-Wide Military Command and Control Systems (WWMCCS), in the highly stressed environments associated with nuclear warfare is an important aspect of the development and deployment of communications systems. In addition to being subject to the physical damage produced by nuclear detonations, communication systems are additionally sensitive to degradation of the propagation medium through which their signals are transmitted. An extensive computational capability has been developed in response to the consequent need to determine the characteristics of propagation degradation and its effects on communications systems. The work reported here addresses one aspect of this degradation that had seemed, until recently, of relatively minor importance. Recognition of circumstances under which propagation degradation has greater significance than formerly thought prompted this examination of its characteristics.

Specifically, we consider the propagation of very-low-frequency (VLF, generally 3 to 30 kHz but here limited to about 10 to 30 kHz) and low-frequency (LF, generally 30 to 300 kHz but here limited to about 30 to 100 kHz) radio signals through regions disturbed by the detonation of many large-yield, near-surface nuclear weapons. Such environments typically arise in the context of large-scale attack scenarios that also include high-altitude detonations. The severity of VLF/LF propagation degradation associated with high-altitude detonations generally is sufficiently great that careful consideration of any additional effects associated with near-surface detonations has in the past been unnecessary. However, at SRI we have recently considered scenarios in which large numbers of large-yield, near-surface detonations occur in areas that are devoid of high-altitude detonations. Furthermore, increasing VLF/LF system margins are making less certain the communications disruption

caused by high-altitude detonations alone, which makes it important to include in the analysis all significant contributors to the propagation disturbance.

The basic mechanism through which nuclear detonations affect VLF/LF propagation is the same for both high- and low-altitude detonations: ionization of the atmosphere in the vicinity of the detonation. This ionization is produced through the interaction of the atmosphere with energetic radiations from the detonation and from its debris. High-altitude detonations tend to illuminate the atmosphere from above because the atmosphere about the burst is too thin for appreciable interaction with it to occur. The radiations from near-surface detonations however, tend to be contained by the atmosphere surrounding the detonation. The radiation-caused ionized regions consequently differ substantially in form for the two detonation types.

The ionization associated with a high-altitude detonation consists of a relatively uniform layer which extends over a large area. The slow lateral variation of this layer permits treatment of its propagation effects in terms of propagation beneath laterally uniform, or stratified, ionization layers. The theory of such propagation has been thoroughly developed. It is this approach that underlies presently available VLF/LF propagation codes.

The ionized region produced by a near-surface detonation is, in contrast, initially confined closely about the burst. Even though the ionized region spreads upward and outward as the debris rises, the lateral variation of the ionization generally precludes an adequate treatment of its propagation effects in terms of propagation beneath stratified layers. The approach adopted in this study to treat this environment is to consider the ambient ionosphere and the additional ionization produced by the detonations as a rough boundary, off which the transmitted signal scatters. Development of this model requires consideration of several factors.

In Section II of this report we examine the characteristics of the ionization produced by near-surface detonations more closely and develop a statistical model of the environment produced by many such detonations. In this model, the environment is characterized by the average number of detonations of a given type that have occurred per unit area. In Section III, we apply the model to determine the perturbation to the coherently reflected component of the signal as a result of the detonations. In Section IV, we examine the characteristics of the energy incoherently scattered by the rough ionospheric reflector. Our conclusions and recommendations are given in Section V.

II PROPAGATION ENVIRONMENT

A. Physical Characteristics

A near-surface nuclear detonation, even of large yield, initially causes significant ionization within only a relatively small volume. The most penetrating radiations immediately produced by the detonation are neutrons and prompt-gamma photons, with ranges of a few hundred of meters at sea level. Thus, the initially ionized region about the detonation has a radius of, at most, a few kilometers. Such regions are too small for a single detonation (or even many detonations separated by distances appreciably exceeding the size of the ionized regions) to affect markedly VLF/LF signals unless either the transmitter or the receiver is located directly adjacent to, or within, such a region.

As a consequence of its radioactivity, however, the debris from the near-surface detonation is also a significant ionization source. This debris rises to substantial altitudes if the yield is sufficiently large. The range of ionizing radiation from the debris generally is greater in the lower-density air of higher altitudes; furthermore, radiation directed upward encounters decreasing air density, and thus increasing range, as it progresses. These factors suffice for the gamma radiation from debris at altitudes above about 20 km to produce an ionized column extending upward from the debris to the ambient lower ionosphere. Altitudes of this order are attained by debris from near-surface detonations with yields greater than about 1 MT. The lateral extent of the debris ionization also grows with increasing altitude since the intensity of the ionizing radiation varies less and less rapidly with lateral distance as the height above the debris increases.

This behavior is illustrated in Figure 1 by contours in a vertical cross section through the detonation point of a constant electron density of 10 cm^{-3} at various times following a 2-MT detonation at 2.5 km altitude.

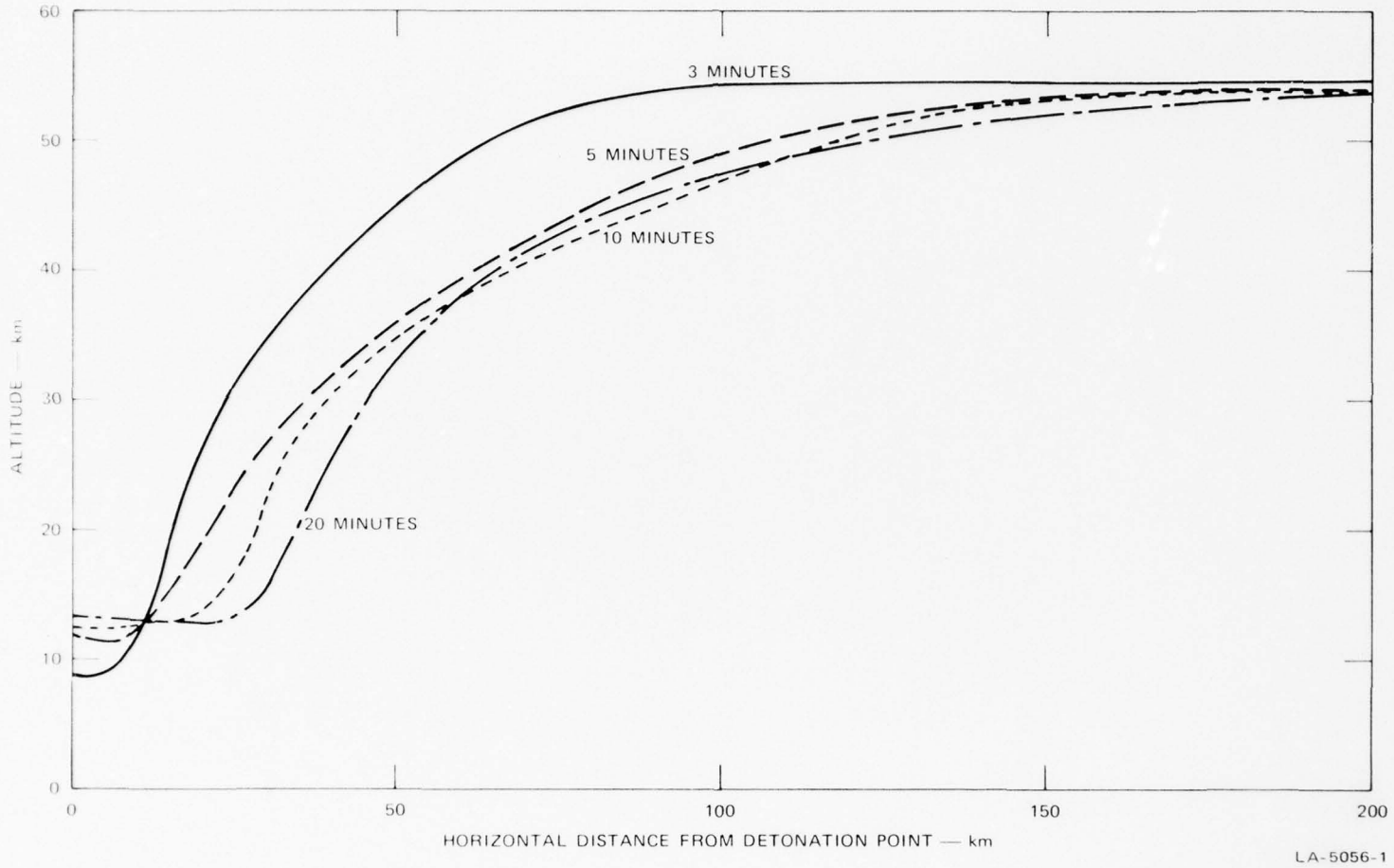

FIGURE 1 PROFILES OF 10 el/cm^3 DENSITY AT VARIOUS TIMES FOLLOWING A LOW-ALTITUDE DETONATION

This ionization level provides a rough indication of a region sufficiently ionized to affect VLF/LF signals. Even 3 minutes following the detonation, the top of the debris cloud has risen sufficiently (about 14-km altitude) to produce significant ionization above it. The debris continues to rise, with some lateral spreading, until about 20 minutes following the detonation. By this time it has stabilized, with its top at an altitude of about 24 km. The size of the ionized region grows until the debris has stabilized; subsequently, the size of the region containing significant ionization may continue to grow as the debris slowly spreads laterally. The ionization intensity gradually subsides, however, as the debris radioactivity diminishes.

Calculation of the effects of debris ionization on a signal involves consideration of both the electrons and the heavier positive and negative ions within the ionized region. A number of simplifying approximations are possible for the altitude ranges of primary interest in this study. At altitudes in the atmosphere below about 70 km, collisions between the ionized species and neutral atmospheric molecules occur with sufficient rapidity that the propagation environment is well described by an isotropic conductivity, σ. The refractive index of the medium, n, is given as a function of the conductivity by

$$n^2 \cong 1 - i \frac{\sigma}{\varepsilon_o \omega} \quad , \tag{1}$$

where ε_o is the permittivity of free space and ω is the wave angular frequency.

In terms of the electron and ion number densities, N_e and N_i respectively,* the conductivity, in turn, is given by

---

* $N_i \equiv 2N_- + N_e$ (N_- the negative-ion density) is the sum of the negative and positive ion number densities. The negative and positive ions are assumed to have approximately equal masses and ion-neutral collision rates.

$$\sigma^2 = e^2 \left(\frac{N_e}{\nu_e m_e} + \frac{N_i}{\nu_i m_i} \right) , \qquad (2)$$

where e is the magnitude of the electron charge, ν_e and ν_i are, respectively, the electron- and ion-neutral collision rates and m_e and m_i are their respective masses. A useful conductivity parameter is the quantity

$$\omega_r \equiv \sigma / \varepsilon_o \quad . \qquad (3)$$

This parameter has been used to characterize the ionization environment in most of the calculations to be described.

Reflection from the ionosphere involves penetration of the incident wave into a medium whose properties do not change sufficiently abruptly to define a precise reflecting surface. It is possible, however, to determine the region in which reflection of the wave primarily occurs. This region is characterized, for altitudes below about 70 km, by values of ω_r that approximate the wave angular frequency, ω. For a wave incident at an angle θ from the vertical, for example, Field and Engel[1] find

$$\omega_r = \sqrt{2}\, \omega \cos^2\theta \qquad (4)$$

provides a useful reference surface within this region.

The precise location of such a surface is not critical if the surface is properly used; we have suppressed the angular dependence in Eq. (4) to simplify matters when considering a range of incidence angles. We generally have used

$$\omega_r = \frac{\omega}{2} \qquad (5)$$

to define a reference surface at altitudes below about 70 km.

In Figure 2, vertical cross sections through such surfaces, as defined by Eq. (5) for a frequency of 20 kHz ($\omega = 4\pi \times 10^4 s^{-1}$ and thus $\omega_r = 2\pi \times 10^4 s^{-1}$), are shown for various times after a 2-MT detonation at 2.5 km-altitude. The corresponding surfaces of constant electron density were illustrated in Figure 1. The constant-conductivity surfaces can be seen generally to have less extreme variation in altitude with distance from the detonation point than do those for 10 el/cm^3. This difference results from the reduced contribution of the electrons to the conductivity at the lower altitudes, where electron collision rate with neutral molecules becomes very high.

If the curvature of the conductivity stratifications within the reflection region is sufficiently small, the relation of reflected to incident wave can be described by the reflection coefficients for an equivalent plane-stratified medium. The planar stratifications of the latter are assumed to be tangent to the curved stratifications of the actual medium in the region of interest. Specifically, to use this approximation it is necessary that[2]

$$k(r_e)_{min} = 2\pi(r_e)_{min}/\lambda > 1 \; ; \tag{6}$$

that is, the product of the minimum radius of curvature of the surface, $(r_e)_{min}$, and the wavenumber, k, must exceed unity.

To evaluate Eq. (6), we note that the product of the two principal (minimum) radii of curvature of a surface, for example r_1 and r_2, is given generally by[2]

$$|r_1\ r_2| = \frac{\left(1 + Z_x^2 + Z_y^2\right)^2}{|Z_{xx}\ Z_{yy} - Z_{xy}^2|} \; , \tag{7}$$

where $Z = Z(x,y)$ is the surface height as a function of the horizontal coordinates x and y. The subscripts denote partial differentiation with respect to the indicated variable or variables. In our case, the heights

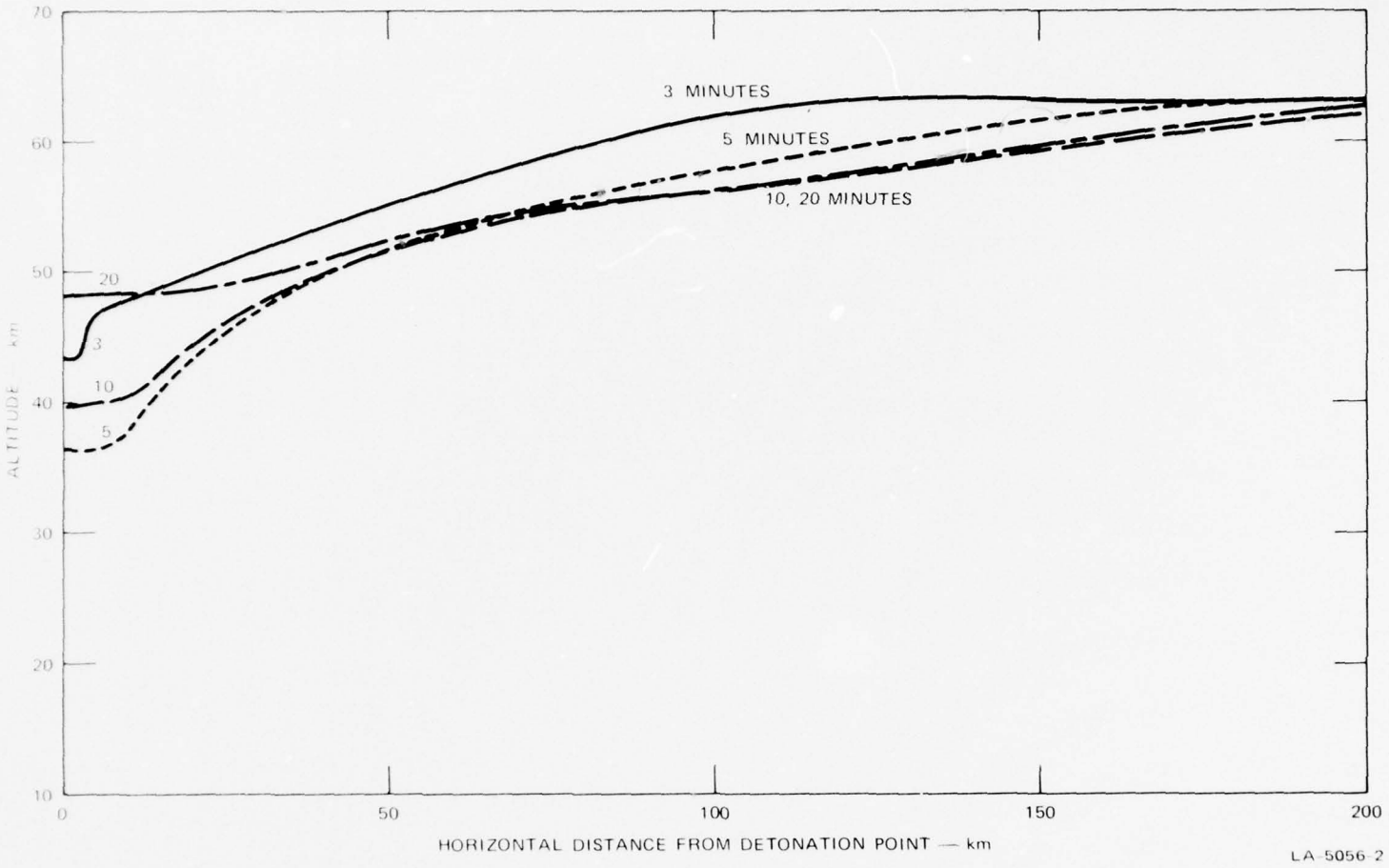

FIGURE 2 PROFILES OF $\omega_r = 2\pi \times 10^4\ s^{-1}$ AT VARIOUS TIMES FOLLOWING A LOW-ALTITUDE DETONATION

of the constant-conductivity strata depend only on the horizontal distance $r = (x^2 + y^2)^{1/2}$ from the detonation point. In terms of r, Eq. (7) becomes

$$|r_1\ r_2| = \frac{r\left(1 + Z_r^2\right)^2}{|Z_{rr}\ Z_r|} \quad . \tag{8}$$

To evaluate r_1 and r_2 separately, we note that one of the principle radii of curvature for an azimuthally symmetric surface will be found along the radial direction. The curvature for this direction is given simply by that of a curve in one dimension: for $Z = Z(r)$ we have[3]

$$r_1 = \frac{\left(1 + Z_r^2\right)^{3/2}}{Z_{rr}} \quad . \tag{9}$$

The other principle radius is then, from Eqs. (8) and (9),

$$r_2 = \frac{r\left(1 + Z_r^2\right)^{1/2}}{|Z_r|} \quad . \tag{10}$$

Table 1 gives values of r_1 and r_2 calculated from Eqs. (9) and (10) for the 3, 5, and 10 minute constant-conductivity contours shown in Figure 2. These conductivity surfaces define reference surfaces for a wave frequency of 20 kHz, or λ = 15 km. Thus, Eq. (6) is satisfied in this case for values of r_e greater than about 2.4 km. Although some scatter results in the values of r_1 and r_2 in Table 1 as a consequence of the relatively coarse distance increments at which the conductivities were determined, these values generally can be seen, with the possible exception of the three-minute case, to support the use of planar reflection coefficients. No difficulties are anticipated at higher frequencies, for which the allowed curvature is even greater, but some caution is indicated in adopting the use of planar reflection coefficients to characterize low-altitude-detonation effects at frequencies below 20 kHz.

Table 1

Principal Radii of Curvature of Constant-Conductivity Surface for 20-kHz Signal

Distance from Detonation (km)	Radii of Curvature					
	At 3 min		At 5 min		At 10 min	
	ρ_1 (km)	ρ_2 (km)	ρ_1 (km)	ρ_2 (km)	ρ_1 (km)	ρ_2 (km)
2	2.5	6.5	50.	67.	151.	35.
5	10.4	8.3	14.5	48.	600.	78.
10	138.	40.	33.	29.	22.	56.
20	580.	97.	94.	46.	126.	57.
50	600.	320.	240.	250.	250.	310.

More complex expressions for the refractive index than Eq. (1) are necessary to characterize the ambient, or near-ambient, nighttime ionosphere, for which ionization levels are too low below 70-km altitude to reflect VLF/LF signals. Definition of a useful reference height is also less straightforward. The signal's interaction with the ionosphere can still be described adequately, however, in terms of planar reflection coefficients, and these coefficients can be readily calculated for this environment as well as the simpler daytime and strongly disturbed environments to which Eqs. (1) and (2) apply.

We have calculated electron and ion densities for detonations representative of those of interest using primarily the weapons-effects phenomenology code WEPH V,[4] which was the most recent version of this continually evolving code available to us at the onset of our study. Some results obtained with its successor, WEPH VI,[5] will also be described briefly. These latter results were obtained in application of the model to a particular environment currently being studied under another DNA contract.* WEPH VI includes improved models of late-time debris spread

* Contract DNA001-77-C-0018.

which are potentially relevant to low-altitude-detonation environments. However, these improvements do not greatly affect the debris behavior during the specific time period to which the greatest attention has been directed in this study, namely the few tens of minutes during which the propagation effects are expected to peak as the debris stabilizes.

B. Statistical Models

Given the means for calculating electron and ion densities in the disturbed environment, the calculation can be very laborious if approached simply as a matter of adding up the contributions to the total ionization production that result from each detonation. An alternative approach has been adopted here to avoid the task of producing a detailed description of the ionization distribution, and consequent propagation effects, caused by different detonation placements. The average effect on propagation of an ensemble of randomly placed detonations will instead be determined; the ensemble is characterized by the average density of detonations per unit surface area. Although some clustering of detonation locations might be anticipated, we here address only the simpler problem of uniformly random detonation placements.

For sufficiently low detonation densities, the regions affected by the individual detonations seldom overlap. If zero overlap is assumed, averages over the ensemble of burst locations can be evaluated to good approximation in terms of an average over the region affected by a single detonation and the fraction of the total surface area that all such regions constitute. For the purpose of illustrative calculations, we have also assumed that all detonations have identical characteristics and occur simultaneously. With these assumptions, calculation of the effects of but a single isolated detonation provides the essential information necessary to evaluate the desired quantities. The limitation to a single type of detonation can readily be relaxed, if necessary, by considering a set of perturbed regions, one for each detonation type.

The region affected by a single detonation can be considered to have a finite area, even though the region is not delimited by a sudden, sharp

cutoff of ionization production. The final result is not sensitive to the specific boundary assumed for this region as long as the region is large enough to encompass the significant detonation effects. The probability density, p(x), for some quantity of interest, x, can then be expressed as a weighted sum of the density for the affected region, $p_D(x)$ and that for the unaffected area, $p_o(x)$;

$$p(x)dx = [\rho A\ p_D(x) + (1 - \rho A)p_o(x)]dx \ , \tag{11}$$

where ρ is the density of detonations per unit surface area, and A is the area of the region taken to be affected by the detonation. It is evident from Eq. (11) that the product ρA must be much less than unity if this approach is to be meaningful, and the contribution of $p_D(x)$ to p(x) will generally be small in such cases.

Averages are similarly constituted:

$$\bar{x} \equiv \int xp(x)dx = \rho A \int_A xp_D(x)dx + (1 - \rho A)\int_{\bar{A}} xp_o(x)dx \ . \tag{12}$$

The probability density for the ambient environment, $p_o(x)$, will generally be a delta function since the quantity x will have some specific value, x_o, for the undisturbed environment. Thus, the right integral in Eq. (12) can be evaluated to give

$$\bar{x} = \rho A \int xp_D(x)dx + (1 - \rho A)x_o \ . \tag{13}$$

This general approach can be extended to detonation densities greater than those to which Eqs. (11) and (13) can be applied, and for which the disturbed effects can indeed become significant. Even when the regions affected by the different detonations overlap appreciably, the area in which two or more detonations contribute similarly to the total ionization often remains only a fraction of the total area of overlap. In the remainder of the overlapping region, the ionizing flux from one of the detonations is markedly more intense than that from the others, and

consideration of only this dominant ionization source should provide a reasonable approximation.

Although we have not evaluated the accuracy of this approximation quantitatively, it appears to be useful to higher detonation densities than might initially be thought to be the case. Consider the horizontal e-folding distance for the ionizing flux from a detonation, which is shorter at lower altitudes than at higher altitudes. The altitude range of interest, and correspondingly the e-folding distance of consequence, decreases with decreasing distance from a detonation. The average linear distance over which dominance in ion production shifts from one detonation to another, in the region midway between two detonations, consequently decreases with increasing detonation density. It is this intermediate region that consideration of only the "dominant" detonation badly mistreats. Thus, the "hardening" of the boundaries between detonations with decreasing separation between them, in reducing the area associated with the boundary region, serves to extend the applicability of the approximation to higher detonation densities than would otherwise have been the case.

An efficient approach to implementation of this model is to determine the probability distribution for the horizontal distance to the nearest detonation. Definition of the functional dependence upon this distance for any quantity of interest then leads immediately to its probability distribution. The distance distribution function derives from the Poisson distribution, which describes the probability for the number of independent events within a region, given their average density. To obtain the distribution, we note that, for small enough regions, the probability that there will be one event within the region becomes the density of events (number per unit area), ρ, times the area of the region, A:

$$P(\text{event in } A) \equiv P(A) = \rho A \quad . \tag{14}$$

Conversely, the probability that there will be no events in A is*

* The probability that there be more than one event in A becomes negligible relative to the probability of one event in A for A sufficiently small.

$$\text{P(no event in A)} \equiv \overline{P(A)} = 1 - \rho A \quad . \tag{15}$$

For areas of appreciable size, we can write

$$\overline{P(A)} = \lim_{N \to \infty} \prod^{N} \overline{P(A/N)} \tag{16}$$

that is, we divide A into N subregions and consider the limit as N becomes large. In this limit, however, the subregions become small, and we can employ Eq. (15) to determine $\overline{P(A/N)}$. Thus, taking $\overline{P(A/N)} = 1 - \rho A/N$, we have, from Eq. (16),

$$\overline{P(A)} = \lim_{N \to \infty} \prod^{N} \left(1 - \frac{\rho A}{N}\right) \quad . \tag{17}$$

Equation (17) is merely one way of defining the exponential function, and we find

$$\overline{P(A)} = e^{-\rho A} \quad , \tag{18}$$

the Poisson distribution for no events in A. For a circular region of radius r, the probability of no detonations within the region is thus

$$\overline{P(r)} = e^{-\pi \rho r^2} \quad . \tag{19}$$

Now, we want to calculate the probability that the nearest burst is at some distance r. For this situation, we require both that no detonations occur at shorter distances and that one occurs at r. These are independent events, so the joint probability is the product of the respective probabilities. Thus, we have, from Eqs. (14) and (19), the probability density function

$$p(r)dr = 2\pi\rho r\, e^{-\pi\rho r^2} dr \tag{20}$$

that the nearest detonation to a point is a distance r from it.

Equation (20) reduces to the expression for isolated detonations, Eq. (11), if the density ρ is sufficiently small. We note that $p(r)dr$ can generally be written

$$p(r)dr = [p(r_1 A) + p(r_1 \bar{A})]dr \quad , \tag{21}$$

where $p(r_1 A)dr$ is the density function for the occurrence of r in A (and $p(r_1 \bar{A})$ the density function for r not in A), and A is now the area affected by a detonation. Equation (21) can equivalently be written, introducing the conditional probabilities $p(r|A)$ and $p(r|\bar{A})$ that r is within or without A respectively, as

$$p(r)dr = [p(r|A)P(A) + p(r|\bar{A})P(\bar{A})]dr \quad . \tag{22}$$

But

$$\begin{aligned} P(A) &= \int_o^{r_A} p(r)dr \\ &= 1 - e^{-\pi\rho r_A^2} \end{aligned} \tag{23}$$

which becomes, for $\pi\rho r_A^2 \ll 1$,

$$P(A) \approx \pi\rho r_A^2 = \rho A \quad . \tag{24}$$

Thus, noting $P(\bar{A}) = 1 - P(A)$,

$$p(r)dr \approx [\rho A p(r|A) + (1 - \rho A)\, p(r|A)]dr \quad . \tag{25}$$

Equation (25) is the equivalent of Eq. (11), since $p(r|A)dr$ and $p(r|\bar{A})dr$ can readily be identified with $p_D(x)dx$ and $p_o(x)dx$, respectively, for $x = x(r)$.

III COHERENT SIGNAL

The roles of the (ideally) smooth earth's surface and lower ionosphere in the propagation of LF/VLF signals around the earth between them can be conveniently expressed in terms of their plane-wave reflection coefficients. These coefficients give the ratio of the field reflected by the boundary to that incident upon it. Decomposition of the signal radiated by the source into an angular spectrum of plane waves, followed by modification of each plane-wave component by the appropriate reflection coefficient(s), yields the field integrals that are evaluated by various presently available computer codes.[6]

The specular, or coherent, reflection from a rough boundary, such as the perturbed ionospheres considered here, can also be described in terms of such reflection coefficients, which, however, now depend on the average properties of the surface.[7] An incoherent return is also built up as a result of scattering of energy out of the specular direction by the surface irregularities. This scattering, which is a function of the variability of the surface properties about their average values, will be discussed further in the next section.

It was shown in Section II-A above, that the perturbed reflecting surfaces produced by debris ionization from the large-yield, low-altitude detonations of interest here have sufficiently large radii of curvature that the interaction with them of the incident field can also be described locally in terms of planar reflection coefficients. This result permits substantial simplification of the calculation of the average reflection coefficients for the perturbed surface--as a first approximation we need only average the local reflection coefficient over the entire surface. A more accurate evaluation, which, however, will not be taken up here, would include modification of the incident-field strength (from that in the unperturbed environment) to account for the possibly significant effects of multiple scatter and shadowing.

Let h' be the height at which ω_r satisfies Eq. (5), and h the reference height chosen for the average reflection coefficient, $R(\theta,h)$, of the rough surface for a plane wave incident at angle θ on the mean surface. Then the average reflection coefficient is given by

$$R(\theta,h) = \int p(r) R_o[\theta,h'(r);r] \exp\left\{i\frac{4\pi\cos\theta}{\lambda}[h - h'(r)]\right\} dr \quad , \quad (26)$$

where $R_o[\theta,h'(r);r]$ is the local reflection coefficient, referenced to height h', and $p(r)$ is given by Eq. (20). The exponential function shifts the phase of R_o from its local reference height h' to the height h, which can appropriately be taken to be the average of the h' over r.

The ionosphere can be separated for low detonation densities into an unperturbed ambient background and nonoverlapping perturbed regions about each detonation, as described in Section II-B, above. The dependence of h' on r within the perturbed region is determined by the shape of the constant-conductivity *surface* for the value of ω_r given by Eq. (5). In the ambient region, h' is a constant. Thus, Eq. (26) becomes

$$R(\theta,h) = 2\pi\rho\int_o^{r_A} r \exp(-\pi\rho r^2) R_o[\theta,h'(r);r] \exp\left\{i\frac{4\pi\cos\theta}{\lambda}[h - h'(r)]\right\} dr$$

$$+ \exp(-\pi\rho r_A^2)\, R_A(\theta,h_A) \exp\left[i\frac{4\pi\cos\theta}{\lambda}(h - h_A)\right] \quad (27)$$

where A is the area of the perturbed region and $R_A(\theta,h_A)$ is the ambient value of R_o, referenced to the ambient height, h_A.

A number of calculations have been made that demonstrate the significance of the detonation effects. Table 2 presents the result of evaluating Eq. (27) for the 20-kHz reflection coefficients of a vertically polarized waves at various times following numbers of 2.5-MT detonations at 2-km altitude in an ambient daytime environment. Results are given for average detonation densities of 0 (ambient), 10^{-6}, 10^{-5}, and 10^{-4} per square kilometer. The nature of the ionospheric perturbation caused by each detonation is illustrated by the constant-electron-density surfaces plotted in Figure 1 and the constant-conductivity surfaces plotted in Figure 2.

Table 2

Average Reflection Coefficients for 20-kHz Vertically Polarized Plane Wave Incident at Angle θ_i in Disturbed Daytime Environment

cos θ_i	Detonation Density (km^{-2})	Reflection Coefficient					
		at 5 minutes		at 10 minutes		at 20 minutes	
		|R|	arg R (deg)	|R|	arg R (deg)	|R|	arg R (deg)
0.1	0	0.675	-160.	0.675	-160.	0.675	-160.
	10^{-6}	0.674	-159.	0.678	-159.	0.676	-158.
	10^{-5}	0.669	-149.	0.687	-149.	0.697	-148.
	10^{-4}	0.571	-117.	0.585	-118.	0.671	-120.
0.2	0	0.453	-144.	0.453	-144.	0.453	-144.
	10^{-6}	0.449	-141.	0.453	-141.	0.453	-140.
	10^{-5}	0.434	-123.	0.458	-121.	0.471	-119
	10^{-4}	0.333	-65.	0.368	-66.	0.435	-66.

The local reflection coefficients were determined for this calculation by fitting exponential gradients at the reference height to the conductivity profiles calculated for different distances from the detonation point. Reflection coefficients for exponential conductivity profiles are available[8] that encompass the range of conductivity gradients found for these profiles. These results were used in a look-up table with interpolation on phase and amplitude between tabulated values to generate the integrand of Eq. (27). The two incidence angles for which calculations were made, 84.3° (cos = 0.1) and 78.5° (cos = 0.2), are representative of the range of angles significant in moderate-to-long distance VLF/LF propagation.

The ambient reflection height, rather than an average height, was used as the phase reference for the disturbed-environment reflection coefficients given in Table 2. With this choice, any change in reflection-coefficient phase from its ambient value is not masked by simultaneous changes in the reference height. An average reference height, however,

would be preferable in any further calculations involving these reflection coefficients.

Aside from some jitter in the results which is caused primarily by the coarseness of the integration step, the data presented in Table 2 show a consistent pattern. Detonation densities below 10^{-6} km^{-2} produce little, if any, effect. At a density of 10^{-5} km^{-2}, the detonations cause a perceptible phase shift and reduction in reflection amplitude at 5 min. The phase shift remains essentially constant between 5 and 20 min, but the amplitude perturbation changes from the reduction at 5 min to an enhancement at 20 min.

The reflection-coefficient perturbation shown by Table 2 for a detonation density of 10^{-4} km^{-2} is substantial. As with that for a density of 10^{-5} km^{-2}, the phase shift remains nearly constant between 5 and 20 min. The reflection amplitude is markedly reduced relative to ambient at 5 min, with the reduction decreasing with increasing time. For $\cos \theta_i = 0.1$, the amplitude appears to have recovered nearly to its ambient value of 20 min. However, the reflection-coefficient behavior for a detonation density of 10^{-5} km^{-2}, coupled with the persistence of the phase perturbation, makes such interpretation suspect; rather, the amplitude perturbation may well evolve into an enhancement at later times before ultimately recovering to its ambient value. At moderate (order of 1000 km) distances, these changes in reflection-coefficient amplitude translate directly into changes in received field strength.

Examination of the reflection coefficients given in Table 2 as a function of $\cos \theta$, the cosine of the incidence angle, shows them to be reasonably well fit by the function form

$$R = - \exp(\alpha \cos \theta) \quad , \tag{28}$$

where $\alpha = \alpha_R + i \alpha_I$ is complex, as illustrated in Figure 3 for the 20-min data. This form has been found to describe well the reflection-coefficient values at grazing incidence angles ($\cos \theta << 1$) for a wide variety of ionospheres.[8,9] Its suitability here makes immediately relevant the VLF

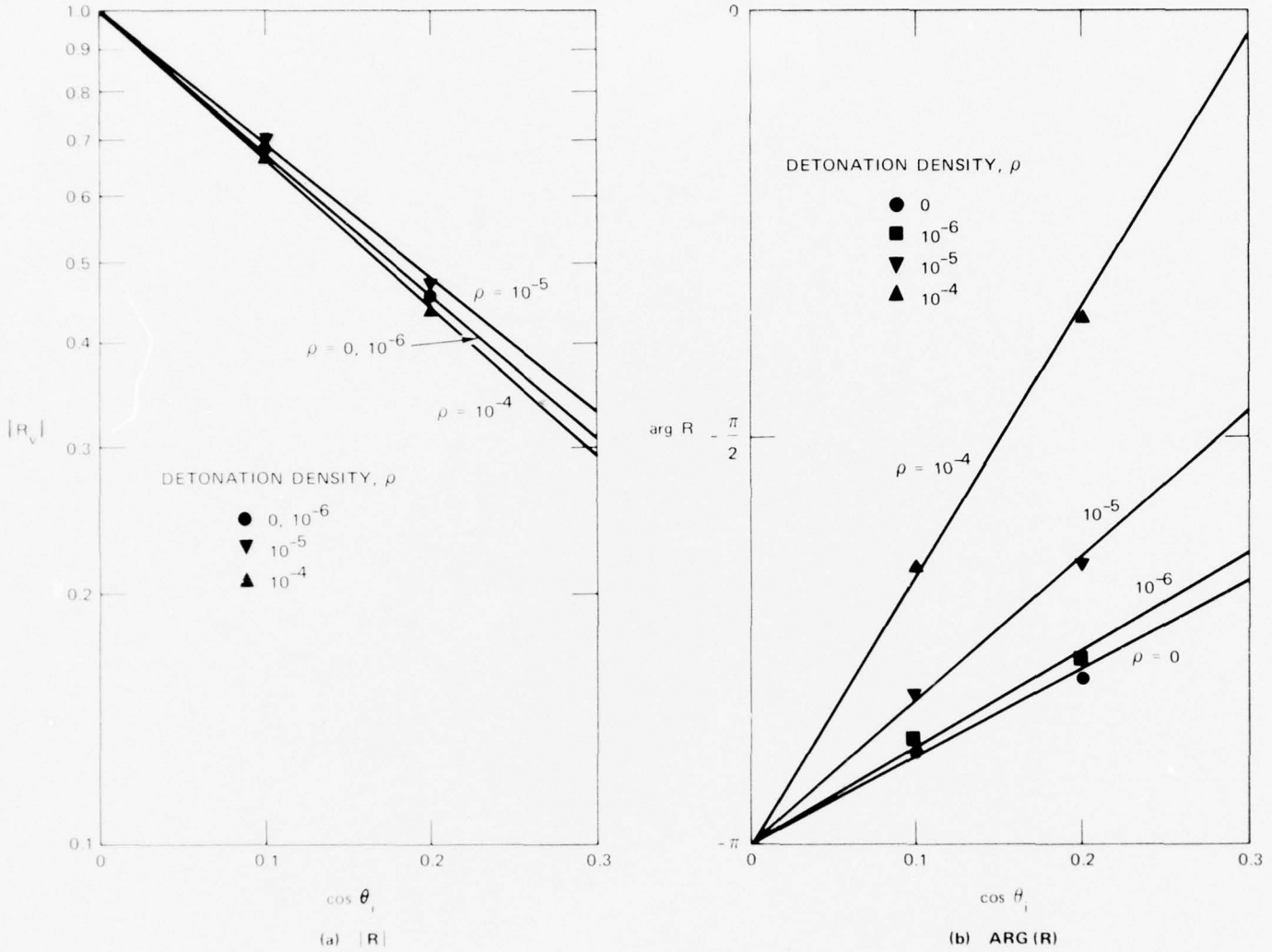

FIGURE 3 DEPENDENCE OF REFLECTION COEFFICIENT ON INCIDENCE ANGLE

modal propagation characteristics calculated by Wait and Spies,[9] which includes parameterization of the results in terms of their dependence on α.

Table 3 gives the values of α derived for the reflection coefficients presented in Table 2. These α, which are an average of the values determined separately from the reflection coefficients for $\cos\theta = 0.1$ and $\cos\theta = 0.2$ in Table 2, yield the linear curves shown in Figure 3. The values of α_I are referenced to a height of 70 km; this height, although somewhat high, is the lowest phase reference height for which modal constants can readily be inferred from Wait and Spies data.[9] Perusal of Wait and Spies results show that the values of α obtained for detonation densities up to 10^{-5} km^{-2} all correspond to attenuation rates over sea water within 0.1 dB of 2.4 dB/Mm, the ambient value. For a detonation density of 10^{-4} km^{-2}, the attenuation rate at 5 min is estimated* to be greater than twice the ambient value, with some recovery, to about twice the ambient value, at 20 min following the detonations. The phase-velocity departures from their ambient value are significant for detonation densities of 10^{-5} km^{-2} or greater.

Table 3

Parameterization of R_v for 20-kHz Wave in the Form

$$R_v = - \exp(\alpha \cos \theta_i)$$

Detonation Density (km^{-2})	α					
	at 5 minutes		at 10 minutes		at 20 minutes	
	α_R	α_I	α_R	α_I	α_R	α_I
0	-3.94	9.35	-3.94	9.35	-3.94	9.35
10^{-6}	-3.97	9.57	-3.92	9.57	-3.94	9.70
10^{-5}	-4.10	11.22	-3.83	11.31	-3.69	11.49
10^{-4}	-5.55	16.55	-5.18	16.42	-4.08	16.24

* The α values for 10^{-4} km^{-2} fall well outside the range of the figures prepared by Wait and Spies,[9] and the necessary extrapolations could be performed only roughly.

Results have also been obtained for propagation in a night environment, as part of a study recently completed under another DNA contract.* Since no night environments were considered in the work performed directly under the contract reported here, some results from this other study will be described briefly.

Night ambient ionospheres do not permit many of the simplifications, described in Section II-A, that are possible for the more intense daytime ionosphere. This greater complexity makes direct numerical calculation of the ionospheric reflection coefficients, using a suitable computer code, perhaps the most straightforward approach to their determination. A version of the procedure developed for such calculations by Pitteway[10] was adopted in this work. The computer code implementing Pitteway's procedure was fed profile data obtained with WEPH VI,[5] the most recent of the WEPH series of nuclear phenomenology codes. The detonation characteristics assumed in this calculation were the same as those adopted for the daytime-environment calculation. The variation of reflection characteristics with horizontal distance from such an isolated detonation in the night environment is exemplified by the data given in Table 4. The entries give the magnitude, at 10 min following such a detonation, of the vertically polarized reflection coefficient, $_{\parallel}R_{\parallel}$, for a 15-kHz wave incident at an angle of 80°. A phase reference height chosen to lie in the reflection region is also indicated in the table. The reference-height criterion used to determine this height reduces to Eq. (4), at low altitudes. Inclusion of the incidence-angle factor of Eq. (4) in the determination of the reference height leads to much lower heights beneath the detonation debris than were obtained for the daytime case, discussed above, using the simplified formula of Eq. (5).

For the night ambient ionosphere, the reflection coefficient of the horizontally polarized wave, $_{\perp}R_{\perp}$, and the conversion coefficients $_{\parallel}R_{\perp}$ and $_{\perp}R_{\parallel}$ must also be known to determine the propagation characteristics; these quantities were all calculated and averaged over the disturbed environment to obtain the necessary data. This calculation was

* Contract DNA001-77-C-0018

Table 4

Reflection Coefficient $\|R\|$ for Vertically Polarized, 15-kHz Wave Incident at 80° on Disturbed Night Ionosphere at 10 Minutes Following a Low-Altitude Detonation

Distance from Detonation (km)	$\|\|R\|\|$	arg $\|\|R\|\|$ (h) (degrees)	Reflection Height h (km)
0	0.513	146.	12.7
15	0.496	141.	12.8
30	0.377	140.	24.4
50	0.384	143.	36.3
75	0.403	146.	44.8
100	0.423	149.	51.0
150	0.446	149.	59.8
200	0.545	154.	66.6
∞	0.461	170.	74.1

repeated for a set of incidence angles that covered the range of values normally significant in VLF propagation, and the averaged reflection coefficients were inserted into a VLF modal propagation code for night environments. Some results of these calculations are given in Table 5 for detonation densities between 10^{-5} and 10^{-4} km^{-2}. The attenuation rate in the undisturbed environment is about 2 dB/Mm.

The night attenuation rates for the disturbed environment given in Table 5 are somewhat larger than the corresponding day rates, as well as representing a greater change from the ambient value than is the case by day. This difference can reasonably be attributed to the greater range of reflection heights, and thus greater phase cancellation in the reflected wave, that occurs at night.

Table 5

Attenuation Rates for 15-kHz Wave Propagating Over Land in Disturbed Night Environment at 10 Minutes Following Detonations

Detonation Density (km^{-2})	Attenuation Rate (dB/Mm)
10^{-5}	3.70
2×10^{-5}	4.80
5×10^{-5}	6.81
10^{-4}	9.73

IV INCOHERENT SIGNAL

A major effect of surface roughness on a signal reflected from the surface is the reduction in amplitude of the coherent, specular return that was discussed in the preceding section. As is evident from the formulation presented there, this amplitude reduction results in large part from phase interference between the contributions to the reflected wave from various parts of the surface. The energy lost from the specular return in this manner is scattered into other directions rather than being absorbed by the boundary.[7] Consequently, it is of interest to determine the incoherent power scattered to the receiver by the surface as well as the strength of the coherent return. For moderate path lengths (up to about 2000 km), multiple reflections between earth and ionosphere play a secondary role in signal propagation. Under these conditions the received signal can be found relatively straightforwardly by direct integration of the contribution from each element of the reflecting surface.

We assume further that (1) multiple scatter between points on the surface can be neglected, (2) the surface curvature is not excessive (as specified by Eq. (6)), and (3) path-length differences for waves scattered from different parts of the surface are sufficiently great to randomize their phases. Under these conditions, integration over the reflecting surfaces can be reduced to a summation of the power scattered by specular points on the surface. A statistical average overall the possible reflecting surfaces then gives the incoherent scattered power as the product of the average number of suitably-oriented specular points per unit surface area, the average scattering cross section of each specular point, and the incident power per unit surface area.[2,3] The average scattering cross section can then be expressed in terms of the average of the product of the principle radii of curvature of the surface at the specular points, a quantity that can be evaluated given knowledge of the surface characteristics.

The specular points are determined by the slope of the rough reflecting surface; i.e., the disturbed ionosphere. The statistics of this surface are used to calculate the average number of specular points per unit area and the averaged product of the principle radii at the specular point. In our statistical model (Section II-B), these characteristics are determined by those of an isolated perturbation, which can be evaluated to whatever precision is required. We have examined in this initial effort only the simplest case of well-separated detonations, for which the isolated-detonation characteristics are related to those of the entire surface by Eq. (11). The incoherent received power in this case is expected, and indeed is found, to be small relative to that in the specular return.

Probability distributions for the reflecting surface slopes are calculated directly from electron and ion contours. Surface characteristics have been determined for 3, 5, 10, and 20 minutes after the detonations occur. Two options for defining the reflecting surface are available in the calculation. The first, and poorer, approximation is to use the height of electron density at 10 el/cm^3 as a function of location. The second option, which provides a more accurate description of the surface, is to use a constant conductivity, the value of which depends on the input frequency, as given by Eq. (5).

Specifically, the rms strength of the vertical component, E_s, of the incoherent field is given by[3]

$$|E_s|^2 = \int_A \frac{\sigma E_I^2 \sin^2\theta_s}{4\pi r'^2} dA \qquad (29)$$

where

E_I = incident field strength at the scattering surface.

σ = scattering cross section per unit surface area.

r' = distance from the scattering element to the reception point.

θ_s = angle between the vertical and the incident ray at the receiver. Because planar geometry is used, this angle is also the projection on a vertical plane through the receiver and the reflection point of the scattered-ray angle at the reflecting surface.

dA = scattering surface increment. The integration is performed over the scattering surface A.

The incident field at the scattering surface is

$$E_I = \frac{V_o \sin \theta_i}{r} \quad , \tag{30}$$

where

r = distance from the transmitter to the scattering element.

V_o = source strength, expressed as a voltage.

$\sin \theta_i$ = pattern factor for radiated field assuming a vertical-dipole source, where

θ_i = angle between the vertical and the ray being transmitted. Because planar geometry is used, this angle is also the projection on a vertical plane through the transmitter and the reflection point of the incident-ray angle at the reflecting surface.

The surface integration is accomplished in polar coordinates. For illustrative purposes, a planar propagation geometry has been chosen, in which Eq. (29) becomes (also using Eq. (30))

$$|E_s|^2 = V_o^2 \int_o^\infty d\rho \, \frac{\rho \sin^2\theta_i(\rho)}{\rho^2 + h^2} \int_o^{2\pi} d\phi \frac{\sigma(\rho,\phi)}{\rho'^2 + h^2} \sin^2\theta_s(\rho,\phi) \tag{31}$$

where

ρ = distance from the transmitter to the point of reflection, measured on the ground plane.

h = average height of the reflecting surface.

ρ' = distance from the receiver to the point of reflection, measured on the ground plane.

The geometry is illustrated in Figure 4.

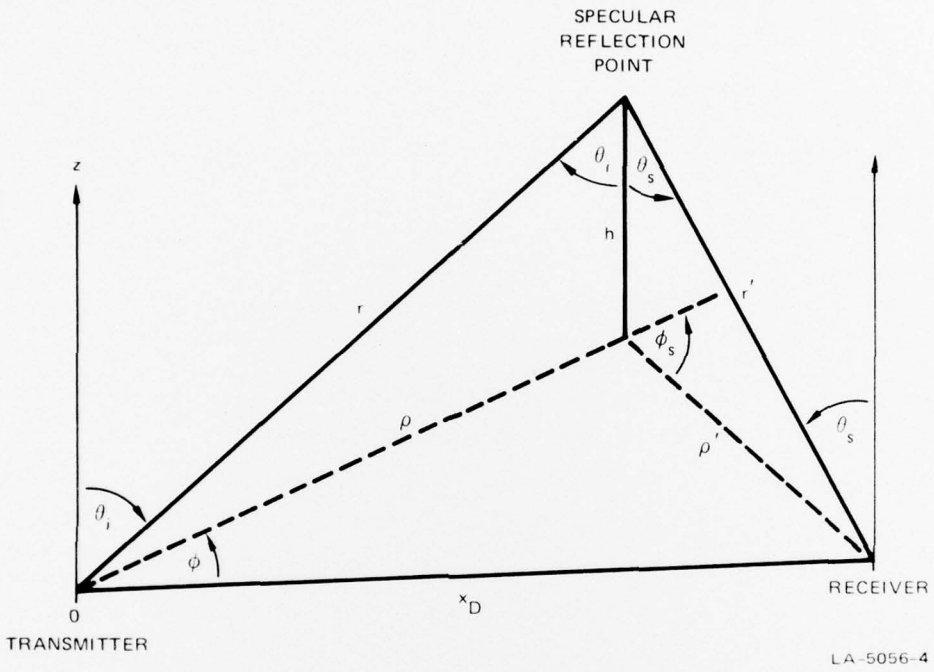

FIGURE 4 INCOHERENT-SCATTER GEOMETRY

The scattering cross section, σ, is obtained from specular-point scatter theory:[2,3]

$$\sigma_{\xi\eta} = \pi n_A \langle |r_1 r_2| \rangle |R_{\xi\eta}(i)|^2 , \qquad (32)$$

where

n_A = average number of specular points per unit area.

$\langle |r_1 r_2| \rangle$ = the average of the product of the principle radii of curvature at the specular points.

$R_{\xi\eta}$ = reflection coefficient for a planar surface tangent to the specular point. The subscripts ξ and η indicate the incident-field and scattered-field polarizations.

Barrick[2] derives the average scattered power as a function of the average number of specular points on the reflecting surface multiplied by the average curvature at these points. He shows that this quantity is equal to the probability density for the slopes necessary to produce a specular point multiplied by an angle factor:

$$n_A \langle |r_1 r_2| \rangle = p(\zeta_x, \zeta_y) \sec^4 \gamma \quad , \tag{33}$$

where

γ = angle between the mean normal to the surface and the local normal to the surface.

ζ = height of the reflecting surface.

ζ_x, ζ_y = surface slope at the specular point; derivatives are in the x and y directions respectively. (ζ_x and ζ_y are computed in a coordinate system where deviations are measured from the average reflecting surface height.)

$p(\zeta_x, \zeta_y)$ = probability of occurrence on the reflecting surface of a point having the slope ζ_x, ζ_y.

Assumptions about the perturbed surface that allow for the analytic simplification are the following:

(1) The burst perturbations are symmetric.

(2) All bursts are identical and occur at once so that all perturbed areas are identical at any specified time.

(3) The effect of a single burst extends over a finite area. The perturbed region has been defined to extend out to the point where the slope becomes less than 0.02. (The ambient reflecting surface has a zero slope in this model.)

(4) The burst locations are represented by a uniform random spatial distribution.

(5) No overlapping bursts are allowed. (The probability of this occurrence is computed as a check.)

If the shape of the perturbed reflecting surface is known, (i.e., ζ_x and ζ_y as a function of x and y) the probability distribution $p(\zeta_x, \zeta_y)$ can be calculated directly from this information, since $p(\zeta_x, \zeta_y)$

is the probability of the joint occurrence of the slope pair ζ_x, ζ_y. The formula for calculating a joint density function is:[11]

$$p(\zeta_x,\zeta_y) = \frac{p(x_1,y_1)}{|J(x_1,y_1)|} + \cdots + \frac{p(x_n,y_n)}{|J(x_n,y_n)|} , \tag{34}$$

where the Jacobian, J, is

$$J(x,y) = \begin{vmatrix} \frac{\partial g(x,y)}{\partial x} & \frac{\partial g(x,y)}{\partial y} \\ \frac{\partial h(x,y)}{\partial x} & \frac{\partial h(x,y)}{\partial y} \end{vmatrix} \tag{35}$$

and the $(x_1,y_1) \ldots , (x_n,y_n)$ are all real solutions of $\zeta_x = 0$ and $\zeta_y = 0$. If we let $g(x,y) = \zeta_x$ and $h(x,y) = \zeta_y$, then substituting in the Jacobian we get:

$$J(x,y) = \begin{vmatrix} \zeta_{xx} & \zeta_{xy} \\ \zeta_{xy} & \zeta_{yy} \end{vmatrix} = |\zeta_{xx}\,\zeta_{yy} - \zeta_{xy}^2| \quad . \tag{36}$$

Since the perturbed reflecting surface is a surface of revolution, according to our assumptions, we change the variables to polar coordinates. The derivatives in Cartesian coordinates in terms of derivatives in polar coordinates are:

$$\zeta_{xx} = \zeta_{rr}\frac{x^2}{r^2} + \zeta_r\frac{y^2}{r^3} = \zeta_{rr}\cos^2\theta + \zeta_r\frac{\sin^2\theta}{r}$$

$$\zeta_{yy} = \zeta_{rr}\frac{y^2}{r^2} + \zeta_r\frac{x^2}{r^3} = \zeta_{rr}\sin^2\theta + \zeta_r\frac{\cos^2\theta}{r}$$

$$\zeta_{xy} = \frac{xy}{r^2}\{\zeta_{rr} - \zeta r/r\} = \{\zeta_{rr} - \zeta r/r\}\sin\theta\cos\theta \quad . \tag{37}$$

The Jacobian turns out to be independent of θ

$$J(x,y) = \left|\zeta_{rr}\ \zeta r/r\right| \quad , \tag{38}$$

and thus

$$p(\zeta_x,\zeta_y) = \frac{p(x_1,y_1)}{\left|\zeta_{rr}(r_1)\ \zeta_r(r_1)/r_1\right|} + \ \ldots\ + \frac{p(x_n,y_n)}{\left|\zeta_{rr}(r_n)\ \zeta_r(r_n)/r_n\right|} \tag{39}$$

with

$$p(x_i,y_i) = 1/\text{area} = 1/(\pi\ R_{max}^2)' \tag{40}$$

where $r_1, \ \ldots\ , r_n$ are solutions of $\zeta_r(r) = 0$.

Because of the nature of the perturbation, we find that each slope occurs at most twice; therefore, n = 2. We also notice that a maximum slope always occurs between the two solutions. The radius of this maximum slope is found prior to any calculation. The solutions of $\zeta_r(r)$ are then localized, and r may be found by iteration. The function $\zeta_r(r)$ is a linear interpolation on data points, and $\zeta_{rr}(r)$ is found analytically from the interpolation formula.

It is important to have a good method of interpolation for the reflecting surface because we are not dealing directly with the surface but with its slope. This quantity is sensitive to minor changes in the method of interpolating between points. The method adopted is relatively simple and introduces very little interpolation error. It is a linear interpolation on the derivative of the surface with respect to the logarithm of the distance. The derivative with respect to logarithmic distance is found directly from the data, which consists of tables of reflecting surface height, ζ, as a function of distance from the center of the burst, r. We have

$$\frac{\partial \zeta_i}{\partial \log r} = \frac{\zeta_{i+1} - \zeta_{i-1}}{\log r_{i+1} - \log r_{i-1}} \quad \text{for } i = 2, \ldots, n-1$$

$$\frac{\partial \zeta_1}{\partial \log r} = \frac{\zeta_2 - \zeta_1}{\log r_2 - \log r_1}$$

$$\frac{\partial \zeta_n}{\partial \log r} = \frac{\zeta_n - \zeta_{n-1}}{\log r_n - \log r_{n-1}} \tag{41}$$

Linear interpolation using logarithmic distance is performed on these smoothed data. Thus

$$\frac{\partial \zeta}{\partial \log r} = \frac{\partial \zeta_{i+1}}{\partial \log r} - \frac{\log r_{i+1} - \log r}{\log r_{i+1} - \log r_i} \left(\frac{\partial \zeta_{i+1}}{\partial \log r} - \frac{\partial \zeta_i}{\partial \log r} \right) \tag{42}$$

for $\log r_i < \log r \leq \log r_{i+1}$, $i = 1, n$, and

$$\zeta_r = \frac{\partial \zeta}{\partial \log r} \frac{\partial \log r}{\partial r} = \frac{\partial \zeta}{\partial \log r} / r \quad . \tag{43}$$

The set of slopes determined this way is integrated to check the agreement with the original reflecting surface. If the smoothing is too severe, additional data points may be added.

A few illustrative calculations have been made using Eq. (31), with V_o chosen to give 1 kW power radiated into a hemisphere over perfectly conducting ground, for numbers of 2.5-km altitude/2-MT detonations, at an average density of 10^{-6} km^{-2}, in the vicinity of a 1000-km daytime path. The effects on the propagation environment of a single such detonation were described in detail in Sections II-A and III. The results of the incoherent-field calculations are summarized in Table 6, from which the root-mean-square (rms) magnitude of the incoherently scattered field is seen to be in the 20 to 40 μV/m range. The fields have been doubled

from the values given directly by Eq. (31) to account for the assumed ground characteristics.

Table 6

Magnitude of RMS Vertical Component of Incoherently Scattered Field at 1000-km Distance from 1-kW Source for a Detonation Density of 10^{-6} km^{-2}

Time After Detonation (m)	$\|E_v\|$ (V/m)		
	at 20 kHz	at 50 kHz	at 100 kHz
3	3.8×10^{-5}	2.3×10^{-5}	2.0×10^{-5}
5	3.4×10^{-5}	2.6×10^{-5}	2.1×10^{-5}
10	3.2×10^{-5}	2.0×10^{-5}	2.3×10^{-5}
20	3.1×10^{-5}	2.2×10^{-5}	2.3×10^{-5}

By comparison, the ambient (coherent) field for one-hop, sky-wave propagation over sea (a highly conducting ground) to the same distance was calculated* to be about 380 μV/m at 20 kHz. Since the coherent field is essentially undisturbed at this detonation density (cf. Table 2), this value--which is approximately 20 dB greater than the largest (3-min) value for the rms incoherent field at this frequency--is also characteristic of the coherent field in the disturbed environment. As we noted above, this smallness of the incoherent field relative to the coherent field is only to be expected at such low detonation densities. This result should not, however, be taken to characterize all cases.

* The ambient field strength was determined using the reflection coefficient given by Eq. (28) for the zero-density angle coefficient σ_R from Table 3, in conjunction with the wave-hop path-integral values obtained by Berry and Chrisman[12] for a 60-km reflection height.

V CONCLUSIONS AND RECOMMENDATIONS

The calculations completed here indicate that high-yield (MT range), low-altitude (few km) nuclear detonations at densities of 10^{-5} km^{-2} or greater have substantial effects on VLF/LF propagation. Such densities of detonations, although high, are not unrealistic for large-scale attack scenarios.

The major effect found at high detonation densities is an increase in the rate of attenuation of the coherently-reflected propagating wave, relative to that in the undisturbed environment, as a result of the ionospheric boundary roughness produced by debris radiations. The consequent attenuation rates are greatest in the disturbed night environment, as a result of the large height range over which reflection occurs for this environment. In contrast to the effects produced by high-altitude detonations, daytime attenuation rates in the disturbed environment are significantly less than those at night.

A method has been presented for determination of the effects of many randomly disturbed detonations in terms of those produced by a single detonation. This method assumes that the effects at all but a small (and to first order negligible) fraction of the affected region are determined primarily by the nearest detonation to each point of the region. Combination of this assumption with a statistical description of the detonation locations greatly simplifies the assessment of the environment. This approach should also be applicable to other types of nuclear effects in addition to that considered here.

A factor not examined quantitatively at significant detonation densities is the fraction of the coherent-signal loss that goes into the incoherently scattered wave. This fraction may not represent a real loss to the communications system under some circumstances. More significantly, the incoherently scattered wave would be expected generally to

remain effective as a jamming signal. Clearly, the distribution of loss between boundary absorption and incoherent scatter, and the utility of the latter as desired and as jamming signal, merits further study.

The calculations reported here must be considered preliminary in several other particulars. Multiple scattering and shadowing have not been taken into account. Further, the accuracy of the statistical model (which expresses the effects of the ensemble of detonations in terms of those of a single detonation) has not been determined. These aspects of the modeling should all be examined and suitable elaboration of the models undertaken if necessary.

Finally, consideration should be given to incorporation of these models, at a suitable level of detail and accuracy, into the DNA nuclear-effects codes for treating VLF/LF propagation.

REFERENCES

1. E. C. Field and R. D. Engel, "The Detection of Daytime Nuclear Bursts Below 150 km by Prompt VLF Phase Anomalies," Proc. IEEE, Vol. 53, pp. 2009-2017 (1965).

2. D. E. Barrick, "Rough Surface Scatter Based on the Specular Point Theory," IEEE Trans. on Antennas and Propagation, Vol. AP-16, pp. 449-454 (1968).

3. R. D. Kodis, "A Note on the Theory of Scattering from an Irregular Surface," IEEE Trans. on Antennas and Propagation, Vol. AP-14, pp. 77-82 (1966).

4. W. S. Knapp, "WEPH V--A Fortran Code for the Calculation of Ionization and Absorption Due to Nuclear Detonations," General Electric Company-TEMPO, Santa Barbara, California, unpublished.

   _____, "WEPH V Code Modifications Through 1 April 1973," General Electric Company-TEMPO, Santa Barbara, California, unpublished.

5. W. S. Knapp and K. Schwartz, "WEPH VI: A Fortran Code for the Calculation of Ionization and Electromagnetic Propagation Effects Due to Nuclear Detonations," General Electric Company-TEMPO, Santa Barbara, California, unpublished.

6. "Summary of VLF and LF Computer Codes," DASA 2212, General Electric Company, Santa Barbara, California (November 1968).

7. P. Beckmann and A. Spizzichino, "The Scattering of Electromagnetic Waves from Rough Surfaces," Ch. 7 (The Macmillan Company, New York, New York, 1963).

8. J. R. Wait and L. C. Walters, "Reflection of VLF Radio Waves from an Inhomogeneous Ionosphere. Part I. Exponentially Varying Isotropic Model," J. Res. NBS, Vol. 67D, pp. 361-367.

9. J. R. Wait and K. P. Spies, "Characteristics of the Earth-Ionosphere Waveguide for VLF Radio Waves," NBS Tech. Note No. 300, Central Radio Propagation Laboratory, National Bureau of Standards, Boulder, Colorado (December 30, 1964).

10. M. L. V. Pitteway, "The Numerical Calculation of Wave-Fields, Reflection Coefficients and Polarizations for Long Radio Waves in the Lower Ionosphere," Phil. Trans. Roy. Soc. (London), Vol. 257, pp. 219-241 (1965).

11. A. Papoulis, Probability Random Variables and Stochostic Processes, p. 201, (McGraw-Hill, New York, New York 1965).

12. L. A. Berry and M. E. Chrisman, "The Path Integrals of LF/VLF Wave Hop Theory," Radio Sci., Vol. 69D, pp. 1469-1480 (1965).

_____, "Numerical Values of the Path Integrals for Low and Very Low Frequencies," NBS Tech. Note No. 319, National Bureau of Standards, Boulder, Colorado (September 2, 1965).

DISTRIBUTION LIST

DEPARTMENT OF DEFENSE

Director
Command Control Technical Center
ATTN: C-650, W. Heidig
ATTN: C-312, R. Mason
ATTN: C-650, G. C. Jones

Director
Defense Advanced Research Proj. Agency
ATTN: Nuclear Monitoring Research
ATTN: TIO, Fred A. Koether

Defense Communication Engineer Center
ATTN: Code 720, John Worthington
ATTN: Code R220, M. Horowitz
ATTN: Code R410, James W. McLean

Director
Defense Communications Agency
ATTN: Code 480
ATTN: Code 810, R. W. Rostron

Defense Documentation Center
Cameron Station
12 cy ATTN: TC

Director
Defense Intelligence Agency
ATTN: DIAAP, Albert L. Wise
ATTN: HQ-TR, J. H. Stewart
ATTN: DT-1BZ, Captain R. W. Morton
ATTN: DIAST-5
ATTN: DB-4C, Edward O'Farrell

Director
Defense Nuclear Agency
3 cy ATTN: RAAE
ATTN: STSI, Archives
ATTN: DDST
3 cy ATTN: STTL, Tech. Library

Dir. of Defense Research & Engineering
Department of Defense
ATTN: S&SS (OS)

Commander
Field Command
Defense Nuclear Agency
ATTN: FCPR

Director
Interservice Nuclear Weapons School
ATTN: Document Control

Director
Joint Strat. Target Planning Staff, JCS
ATTN: JPST, Captain G. D. Goetz

Chief
Livermore Division, Field Command, DNA
Lawrence Livermore Laboratory
ATTN: FCPRL

DEPARTMENT OF DEFENSE (Continued)

Director
National Security Agency
ATTN: Oliver H. Bartlett, W32
ATTN: John Skillman, R52

OJCS/J-3
ATTN: WWMCCS, Eval. Ofc., Mr. Toma

Director
Telecommunications & Comd. & Con. Sys.
ATTN: Asst. Dir. (Sys.)
ATTN: Scientific Advisor

DEPARTMENT OF THE ARMY

Commander/Director
Atmospheric Sciences Laboratory
US Army Electronics Command
ATTN: DRSEL-BL-SY-S, F. E. Niles

Commander
Harry Diamond Laboratories
ATTN: DRXDO-NP, Francis N. Wimenitz
ATTN: DRXDO-TI, Mildred H. Weiner

Director
US Army Ballistic Research Labs.
ATTN: Tech. Lib., Edward Baicy

Commander
US Army Electronics Command
ATTN: J. E. Quigley

Commander
US Army Foreign Science & Tech. Center
ATTN: P. A. Crowley
ATTN: R. Jones

Commander
US Army Materiel Dev. & Readiness Command
ATTN: DRCLDC, J. A. Bender

Commander
US Army Nuclear Agency
ATTN: MONA-WE, J. Berberet

DEPARTMENT OF THE NAVY

Chief of Naval Operations
Navy Department
ATTN: OP 943, LCDR Huff

Chief of Naval Research
Navy Department
ATTN: Code 461
ATTN: Code 421
ATTN: Code 402
ATTN: Code 420

Commander
Naval Electronic Systems Command
Naval Electronic Systems Command Hqs.
ATTN: PME 117

PRECEDING PAGE NOT FILMED
BLANK

DEPARTMENT OF THE NAVY (Continued)

Commanding Officer
Naval Intelligence Support Center
ATTN: Code 5404, J. Galet

Commander
Naval Ocean Systems Center
3 cy ATTN: Code 2200, W. F. Moler
ATTN: R. Eastman

Director
Naval Research Laboratory
ATTN: Code 5461
ATTN: Code 5465
3 cy ATTN: Code 7701, Jack D. Brown
ATTN: Code 5460, Radio Electromag Prop. Br.
ATTN: Code 5430

Commander
Naval Surface Weapons Center
ATTN: Code WA501, Navy Nuc. Prgms. Off.

Director
Strategic Systems Project Office
Navy Department
ATTN: NSP-2141

DEPARTMENT OF THE AIR FORCE

Commander
ADC/DC
ATTN: DC, Mr. Long

Commander
ADCOM/XPD
ATTN: XPQDQ

AF Geophysics Laboratory, AFSC
ATTN: SUOL, Research Lib.
ATTN: CRU, S. Harowitz
ATTN: OPR, James C. Ulwick
ATTN: OPR, Alva T. Stair

AF Weapons Laboratory, AFSC
ATTN: SUL
ATTN: DYC, Captain L. Wittwer
ATTN: NSS

AFTAC
ATTN: TN
ATTN: TF/Major Wiley

Air Force Avionics Laboratory, AFSC
ATTN: AFAL AAB, H. M. Hartman

Headquarters
Electronic Systems Division, AFSC
ATTN: James Whelan

Hq. USAF/RD
ATTN: RDQSM

Commander
Rome Air Development Center, AFSC
ATTN: EMTLD, Doc. Library

SAMSO/SZ
ATTN: SZ
ATTN: SZJ, Major Lawrence Doan

DEPARTMENT OF THE AIR FORCE (Continued)

Commander In Chief
Strategic Air Command
ATTN: Chief Scientist
ATTN: XPFS, Major Brian G. Stephan
ATTN: ADWATE, Captain Bruce Bauer

ENERGY RESEARCH & DEVELOPMENT ADMINISTRATION

Division of Military Application
US Energy Research & Dev. Admin.
ATTN: Doc. Control for Donald I. Gale

University of California
Lawrence Livermore Laboratory
ATTN: Frederick D. Seward, L-46
ATTN: Glenn C. Werth, L-216

Los Alamos Scientific Laboratory
ATTN: Doc. Con. for J. H. Coon
ATTN: Doc. Con. for R. F. Taschek
ATTN: Doc. Con. for P. W. Keaton
ATTN: Doc. Con. for Donald R. Westervelt

Sandia Laboratories
Livermore Laboratory
ATTN: Doc. Con. for Byran E. Murphey
ATTN: Doc. Con. for Thomas B. Cook, Org. 8000

Sandia Laboratories
ATTN: Doc. Con. for Space Project Div.
ATTN: Doc. Con. for 3141 Sandia Rpt. Coll.
ATTN: Doc. Con. for A. Dean Thornbrough, Org. 1245

US Energy Research & Dev. Admin.
Albuquerque Operations Office
ATTN: Doc. Con. for D. W. Sherwood

US Energy Research & Dev. Admin.
Division of Headquarters Services
Library Branch G-043
ATTN: Doc. Con. for Allen Labowitz

OTHER GOVERNMENT AGENCIES

Department of Commerce
National Bureau of Standards
ATTN: Raymond T. Moore
ATTN: Arthur Ernst

Department of Commerce
Office of Telecommunications
Institute for Telecom Science
ATTN: William F. Utlaut

Department of Transportation
Office of the Secretary
ATTN: R. L. Lewis
ATTN: R. H. Doherty

DEPARTMENT OF DEFENSE CONTRACTORS

Aeronomy Corporation
ATTN: S. A. Bowhill

Aerospace Corporation
ATTN: Irving M. Garfunkel

DEPARTMENT OF DEFENSE CONTRACTORS (Continued)

Analytical Systems Engineering Corp.
ATTN: Radio Sciences

The Boeing Company
ATTN: J. F. Kenny
ATTN: Glenn A. Hall

University of California at San Diego
ATTN: Henry G. Booker

ESL, Inc.
ATTN: James Marshall

General Electric Company
TEMPO-Center for Advanced Studies
ATTN: DASIAC
ATTN: Don Chandler

GTE Sylvania, Inc.
Electronics Systems GRP-Eastern Div.
ATTN: Marshal Cross

Johns Hopkins University
Applied Physics Laboraoty
ATTN: Document Librarian

Lockheed Missiles & Space Company, Inc.
ATTN: Richard G. Johnson, Dept. 52-12

Lowell Technol. Inst. Research Foundation
ATTN: Dr. Bibl

DEPARTMENT OF DEFENSE CONTRACTORS (Continued)

M.I.T. Lincoln Laboratory
ATTN: Lib. A-082 for David M. Towle
ATTN: L-246, James H. Pannell

Mission Research Corporation
ATTN: R. Hendrick
ATTN: M. Scheibe
ATTN: F. Fajen

The Mitre Corporation
ATTN: John Morganstern
ATTN: G. Harding

Pacific-Sierra Research Corp.
ATTN: E. C. Field, Jr.

Pennsylvania State University
Ionosphere Research Laboratory
ATTN: Ionospheric Research Lab.

R & D Associates
ATTN: William J. Karzas
ATTN: Bryan Gabbard
ATTN: R. P. Turco
ATTN: H. A. Ory

The Rand Corporation
ATTN: Cullen Crain

Stanford Research Institute
ATTN: Donald Neilson
ATTN: Walter G. Chesnut
ATTN: James R. Peterson
ATTN: Gary H. Price
ATTN: V. Elaine Hatfield

Division of Vitro Laboratories
Automation Industries, Inc.
ATTN: David Hill